Check for updates

ADVANCED FUNCTIONAL MATERIALS
www.afm-journal.de

Fluorinated Aromatic Anode-electrolyte Interface for Highly Reversible Zinc Anode

*Tao Shen, Changyuan Li, Yifan Wang, Zhaoqian Li, Menghao Yang, Long Yang, and Chaofeng Liu**

The issues of dendrite formation and side reactions at the zinc anode–electrolyte interface are the primary factors limiting the reversibility and stability of aqueous zinc-ion batteries (AZIBs). Herein, the functionalities of fluorinated aromatic additive on zinc anode–electrolyte interface are investigated by comparing a series of organics with N-, phenyl-, and F-groups individually or jointly. An additive, 3-(trifluoromethyl)-phenyltrimethyl-ammonium bromide (TFPM), featuring the hydrophobic groups from benzene ring and fluorine together, effectively regulates zinc ion deposition to prevent dendrite formation. It also isolates high-activity water during the desolvation process and forms a robust solid electrolyte interphase (SEI) layer to suppress interfacial parasitic reactions. As a result, Zn//Zn symmetric batteries with TFPM additive exhibit an ultralong cycling lifetime over 5900 h (over 8 months) at 0.5 mA cm^{-2}, and improved Coulombic efficiency (CE) of 99.93% over 4000 h at 1 mA cm^{-2} than bare $ZnSO_4$ electrolyte in Zn//Cu symmetric batteries. Paring with Mn^{2+} preintercalated $V_2O_5{\cdot}nH_2O$ cathode (MnVO), the full battery delivers a high capacity of 263 mAh g^{-1} at 8 A g^{-1} with a retention of 94.9% over 6000 cycles. This work provides a promising interface-engineering strategy from the functional group design of additives for high-performance AZIBs.

1. Introduction

Aqueous zinc-ion batteries (AZIBs) have garnered significant attention due to their unique advantages, including the relatively low redox potential of zinc metal (−0.76 V vs. SHE), high theoretical capacity (820 mAh g^{-1} or 5855 mAh cm^{-3}), abundant resource availability, and high safety, presenting their great potential as one of the most promising sustainable energy storage devices.[1] However, dendrite growth and side reactions at the zinc–electrolyte interface not only shorten the cycling lifespan and reduce the CE of the battery but also increase the risk of battery swelling, leakage, and separator puncture, potentially leading to short circuits.[2] These issues are primarily attributed to the uneven charge distribution on the zinc surface and the highly reactive water molecules involved in the desolvation process. The uneven charge distribution, caused by the inherent surface irregularities of Zn plates, could induce preferential zinc ion deposition at the protrusions, a phenomenon known as the "tip effect".[3] Additionally, the desolvated water molecules located in the electric double layer (EDL), characterized by high thermodynamic activity, could severely corrode Zn metal, accelerate the hydrogen evolution reaction (HER), and induce the formation of zinc hydroxide sulfate (ZHS).[4] These two issues mutually interfere, further restricting their potential applications in energy storage.[5]

Extensive efforts have been dedicated to improving the reversibility and stability of the Zn anode, including separator modification,[6] low-lattice mismatch substrates,[7] Zn metal structure design,[8,9] and electrolyte optimization.[10] Among these strategies, electrolyte optimization has emerged as a particularly promising approach due to its simplicity, high efficiency, and low cost.[11] Reducing the water content in the Zn ion solvation sheath, a key approach in electrolyte optimization becomes an effective and efficient way to mitigate side reactions because the highly reactive water is replaced by molecular additives in the chemical coordination surrounding zinc ions.[4b,12] However, side reactions cannot be fundamentally and completely suppressed due to the limited coordination sites in the solvation sheath. The EDL at the zinc anode-electrolyte interface plays a critical role in governing the desolvation and reduction processes of zinc anodes,[13] thereby fundamentally determining the electrochemical performance of aqueous zinc-ion batteries. Constructing an H_2O-poor EDL structure would be advantageous for isolating water from the zinc metal, offering a dendrite-free and HER-free zinc redox process.[14] The aforementioned functions require

T. Shen, C. Li, M. Yang, L. Yang, C. Liu
Interdisciplinary Materials Research Center
School of Materials Science and Engineering
Tongji University
Shanghai 201804, P. R. China
E-mail: chaofeng@tongji.edu.cn
Y. Wang, Z. Li
Key Laboratory of Photovoltaic and Energy Conservation Materials
Institute of Solid State Physics
Hefei Institutes of Physical Science
Chinese Academy of Sciences
Hefei, Anhui 230031, P. R. China
Y. Wang
University of Science and Technology of China
Hefei, Anhui 230026, P. R. China

The ORCID identification number(s) for the author(s) of this article can be found under https://doi.org/10.1002/adfm.202509705

DOI: 10.1002/adfm.202509705

 © 2025 Wiley-VCH GmbH

16163028, 2025, 47, Downloaded from https://advanced.onlinelibrary.wiley.com/doi/10.1002/adfm.202509705 by Tongji University, Wiley Online Library on [24/12/2025]. See the Terms and Conditions (https://onlinelibrary.wiley.com/terms-and-conditions) on Wiley Online Library for rules of use; OA articles are governed by the applicable Creative Commons License

additives with strong zincophilicity. Generally, elements with high electronegativity (such as O, S, N, F) possess a strong ability to attract electrons, thus organic molecules containing functional groups like (N-, F-) prefer to adsorb on zinc metal.[15] In addition, the benzene ring, a hydrophobic functional group, is prone to form stable adsorption states with metals due to the interaction between its π-electrons and the metal's *d*-orbital electrons.[16] In addition to the effective adsorption, the partial decomposition of additives forms SEI that could enhance the interfacial stability during cycling.[17] According to molecular orbital theory, molecules with the lower LUMO (lowest unoccupied molecular orbital) energy levels are preferentially reduced by gaining electrons at the anode surface rather than the decomposition of water, resulting in SEI formation. The well-constructed SEI can provide zincophilic sites for uniform metal deposition and inhibit HER.[18] Fluorinated SEI engineering has been demonstrated to effectively suppress side reactions and dendrite formation, thereby enhancing the stability of the zinc anode-electrolyte interface.[19] Therefore, it is essential to explore multifunctional additives capable of simultaneously establishing an H_2O-poor EDL and a stable and robust fluorinated SEI to achieve high-performance AZIBs.

In this work, a series of organics with different functional groups are systematically investigated to verify their respective and synergistic effects. An additive, 3-(trifluoromethyl)phenyltrimethyl-ammonium bromide (TFPM), with the hydrophobic groups of benzene ring and fluorine together, has been proven to be the best interfacial stabilizer in $ZnSO_4$ (denoted as ZSO) electrolyte. Density functional theory (DFT) calculations suggest that the adsorption energy of $TFPM^+$ on the zinc surface is higher than that of H_2O molecules, facilitating the formation of H_2O-poor EDL to inhibit HER at the Zn metal surface. The adsorbed $TFPM^+$ also regulates the diffusion of Zn ions at the anode-electrolyte interface, inducing stacked layered growth and a preferred Zn(002) texture. Besides, the partial TFPM cation decomposes to form a ZnF_2-rich SEI layer, effectively suppressing side reactions at anode-electrolyte interface and regulating the transport of Zn^{2+} toward the electrode surface for the ZnF_2 has been demonstrated to exhibit high ionic conductivity.[20] Taking advantage of this H_2O-poor EDL and stable SEI layer, Zn//Zn symmetric batteries using TFPM/ZSO electrolyte deliver an ultra-long cycle life of 5900 h at a current density of 0.5 mA cm^{-2} with an areal capacity of 0.5 mAh cm^{-2}. Using Zn//Cu half batteries tested in the TFPM/ZSO electrolyte, a high CE of 99.93% is achieved at 1 mA cm^{-2} and 0.5 mAh cm^{-2}, indicating the excellent reversibility of the Zn plating–stripping process. The synergistic effects of TFPM are further demonstrated in the Zn-MnVO full batteries with a stable cycle lifespan over 6000 cycles and higher capacity retention of 94.9% at 8 A g^{-1}.

2. Results and Discussion

To reveal the functionality and synergy of the functional groups in the additives, three additives with N-, phenyl-, and F- groups individually or jointly are investigated. Firstly, the adsorption energies of the Zn atom, H_2O molecule, tetramethylammonium bromide (TM^+), trimethylphenylammonium bromide (TPM^+), and $TFPM^+$ cations on Zn (002) facet are calculated using first-principles calculations. The molecular structure and adsorption model of TM^+, TPM^+, and $TFPM^+$ are shown in **Figure 1a**. Figure 1b compares the adsorption energies of these species on the Zn(002) facets. $TFPM^+$ presents the largest adsorption energy (absolute value) of −2.64 eV with Zn, manifesting the most preferential affinity. The increasing adsorption energies of TM^+, TPM^+, and $TFPM^+$ suggest the synergistic contribution of phenyl- and trifluoromethyl- and fluorine groups to enhance their interaction with Zn anode. Tafel curves in Figure 1c verify that TFPM/ZSO electrolyte exhibits the lowest corrosion current (0.103 mA cm^{-2}) and the highest corrosion potential (16 mV) compared to other electrolytes, indicating the alleviated Zn corrosion. The linear sweep voltammetry (LSV) results in Figure 1d show the lowest hydrogen evolution potential of 80 mV in TFPM/ZSO electrolyte than other electrolytes, suggesting the $TFPM^+$ inhibits HER. The chronoamperometry (CA) results (Figure 1e) show the continuously increasing current density for over 150 s in the ZSO electrolyte, indicating that the Zn deposition is mainly primarily governed by a typical 2D diffusion process. This phenomenon is attributed to inhomogeneous zinc deposition behavior and dendritic Zn formation caused by the "tip effect".[3c] In contrast, the initial decrease in current density originates from the adsorption of additives on the zinc surface in TM/ZSO, TPM/ZSO, and TFPM/ZSO electrolytes. TFPM/ZSO electrolyte presents a stable and constant 3D diffusion after a short 2D diffusion within 20 s. It is attributed to TFPM with higher adsorption energy towards zinc, enabling rapid and stable adsorption on the anode surface. Such strong interfacial interaction effectively regulates Zn^{2+} deposition. However, the current densities increase in TM/ZSO and TPM/ZSO after 20 s. This is attributed to the low adsorption energies of TM and TPM on the zinc anode surface, resulting in insufficiently stable adsorption that renders them prone to detachment. Consequently, the current density progressively increases, exhibiting a 2D diffusion behavior. The confocal laser scanning microscope (CLSM) images in Figures 1f–i show that the zinc anode in TFPM/ZSO electrolyte exhibits more compact and flat deposition, and the statistical height distribution of Zn-deposit is also more centralized compared to other electrolytes (Figures 1j–m). Considering the comprehensive impacts of electrolyte additives, the optimal concentration of TFPM is 10^{-3} M (Figures S1–S4).

Figure 2a shows $TFPM^+$ with a higher HOMO (highest occupied molecular orbital) and lower LUMO energy levels compared to H_2O. Electrostatic potential (ESP) map analysis suggests $TFPM^+$ with lower charge density, indicating a greater tendency to attract electrons and interact with zinc metal (Figure 2b). The contact angle of TFPM/ZSO electrolyte is 77.8° on Zn metal, much lower than 93.2°of ZSO bare electrolyte (Figure 2c), suggesting $TFPM^+$ added electrolyte with better wettability and zincophilic properties. The ab initio molecular dynamics simulation (AIMD) shows that the Zn−F bond between $TFPM^+$ and the Zn surface remains stable after 3 ps, demonstrating a stable adsorption (Figure S5). The Zn metal electroplated in the TFPM/ZSO electrolyte at a current density of 5 mA cm^{-2} for 1 h, the presence of the characteristic N1*s* and F1*s* peaks and the positive shift of the Zn 2p peak in the X-ray photoelectron spectroscopy (XPS) results confirm the adsorption behavior of $TFPM^+$ on Zn metal surface (Figures 2d,e). The C 1*s* spectrum in the XPS has been

 © 2025 Wiley-VCH GmbH

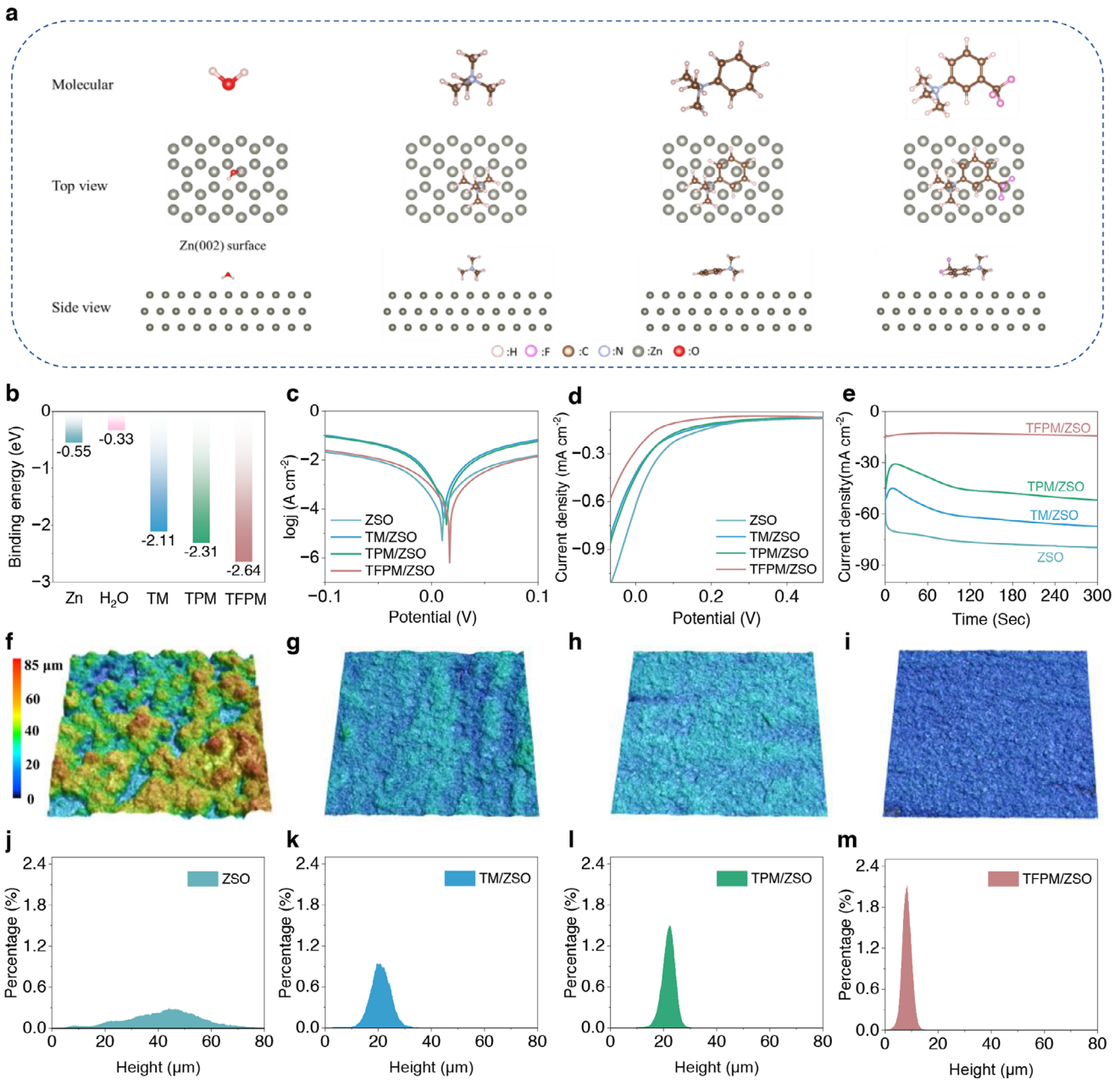

Figure 1. a) Optimal adsorption configuration for Zn atom, H_2O molecule, TM^+, TPM^+, and $TFPM^+$ cations on the Zn (002) facet. b) The adsorption energies of the species on the Zn (002) facet. (c) Tafel curves, (d) LSV curves, and (e) CA curves of Zn metal in different electrolytes. f–i) CLSM images of the Zn metal after deposition in (f) ZSO, (g) TM/ZSO, (h) TPM/ZSO, (i) TFPM/ZSO electrolytes at a current density of 10 mA cm^{-2} for 1 h. j–m) The statistical height distribution of Zn deposit in (j) ZSO, (k) TM/ZSO, (l) TPM/ZSO, (m) TFPM/ZSO electrolytes.

charge-corrected to guarantee the reliability of the Zn peak shift (Figure S6). The electrokinetic (Zeta) potential measurements confirm the strong electrostatic adsorption of $TFPM^+$ on the Zn surface, as evidenced by the positive shift in potential from −1.88 to −0.41 mV compared to bare ZSO electrolyte (Figure 2f). The decreased capacitance in Figure 2g indicates that $TFPM^+$ regulates the EDL structure, demonstrating its preferentially strong adsorption with Zn metal. The higher nucleation overpotential in the TFPM/ZSO electrolyte further validates an additional energy for constructing EDL and a restrained nucleation process (Figure 2h and Figure S7).[10c] These results above demonstrate that the adsorption of $TFPM^+$ on the Zn surface constructs an H_2O-poor EDL structure at the Zn anode-electrolyte interface. $TFPM^+$ adsorbed on zinc surfaces strengthens the repulsion of hydrated Zn ions at EDL to inhibit hydrogen evolution and corrosion by isolating the active H_2O molecules in the solvent sheath and the zinc anode surface. The positively charged $TFPM^+$ also tends to accumulate at the tips of electron-rich protrusions, forming a dynamic electrostatic shielding layer that homogenizes the local surface electric field to suppress the "tip effect". Moreover,

© 2025 Wiley-VCH GmbH

16163028, 2025, 47, Downloaded from https://advanced.onlinelibrary.wiley.com/doi/10.1002/adfm.202509705 by Tongji University, Wiley Online Library on [24/12/2025]. See the Terms and Conditions (https://onlinelibrary.wiley.com/terms-and-conditions) on Wiley Online Library for rules of use; OA articles are governed by the applicable Creative Commons License

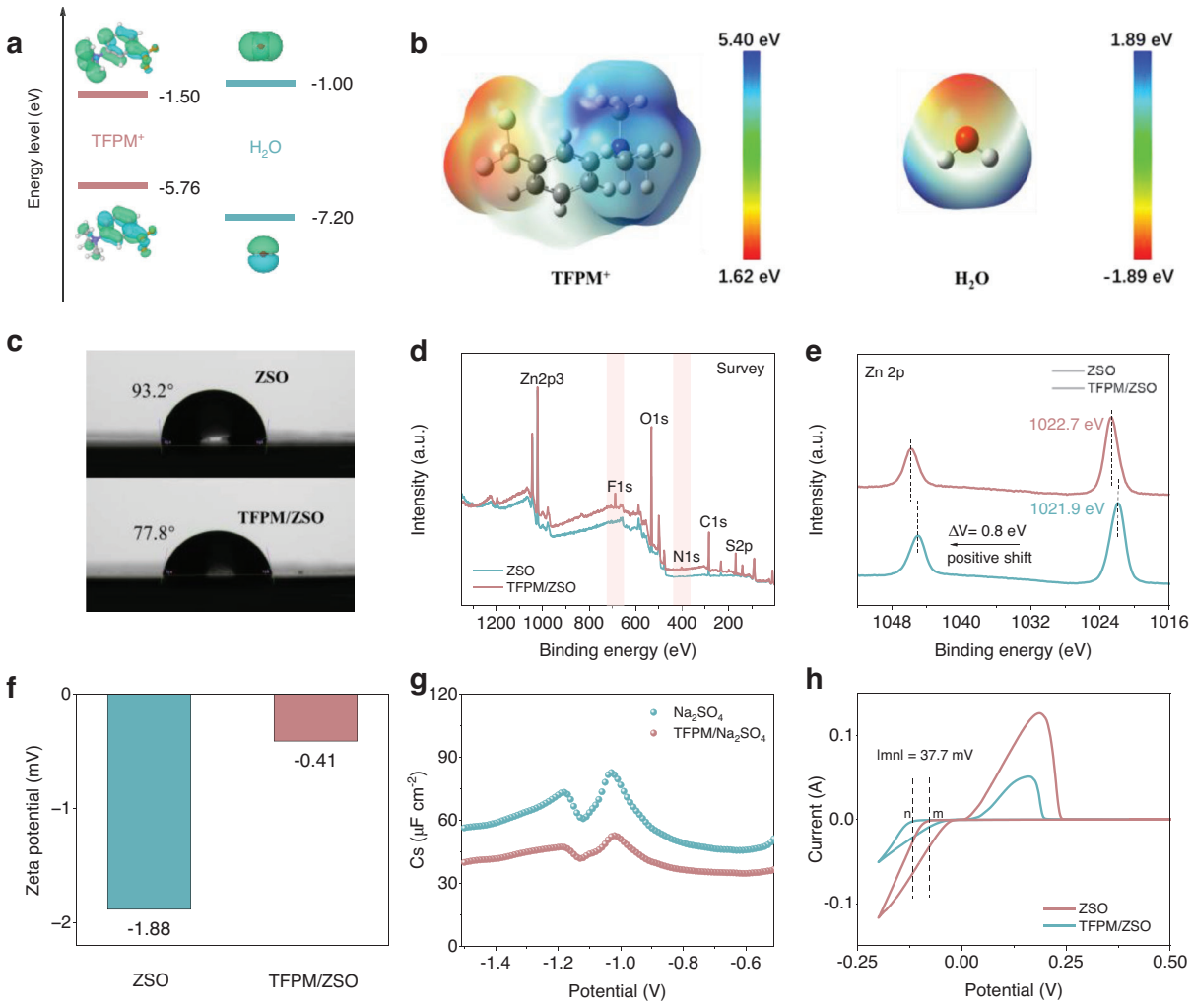

Figure 2. a) LUMO and HOMO isosurfaces of $TFPM^+$ and H_2O molecule. b) ESP maps of $TFPM^+$ and H_2O molecule. c) Contact angles of Zn metal with different electrolytes. d) XPS survey and e) Zn 2*p* spectra of Zn anodes after electroplating for 1 h in different electrolytes. f) Zeta potentials of Zn powders in different electrolytes. g) Differential capacitance curves for Zn metal in Na_2SO_4 solution with and without TFPM additive. h) The nucleation potential in CV tests of Zn//Cu batteries with different electrolytes at the scan rate of 1 mV s^{-1}.

the (002) facet exhibits the highest adsorption energy (absolute value) for $TFPM^+$, which significantly reduces the deposition rate on this facet. As a result, zinc preferentially deposits along the (002) facet, leading to the formation of plate-like zinc structures.

Zn anode presents less byproducts in TFPM/ZSO than in bare ZSO electrolytes after plating–stripping as shown in **Figure 3**a. Besides, the zinc anode exhibits a characteristic (002) texture, indicating that $TFPM^+$ regulates the deposition behavior of zinc ions. Time-dependent X-ray Diffraction (XRD) patterns show the intensity ratio between (002) and (100) facets (denoted as $R = I_{002}/I_{101}$) (Figure 3b,c) continuously increases from 0.42 to 7.21 with the deposition time increase. The progressively increasing *R* ()value is associated with a greater exposure of the Zn(002) facet. SEM images in Figure S8 show that the electrodeposited Zn metal consists of hexagonal Zn plates with an epitaxial microstructure, corresponding to the Zn(002) crystal facet parallel to the Zn substrate. These results indicate that $TFPM^+$ benefits promote the preferential growth of the (002) facet. X-ray diffraction pole figures also demonstrate the Zn plate deposited in the ZSO electrolyte manifests a widely distributed signal for (002) with lower intensity (Figure 3d). In contrast, the concentrated distribution and higher intensity in TFPM/ZSO verify the formation of a predominant (002) facet (Figure 3e). To investigate the underlying deposition mechanism, ab initio calculations based on DFT in Figure 3f show that the adsorption energy (absolute value) of $TFPM^+$ (−2.64 eV) on Zn(002) facet is highest than that on (100) and (101) facets (−1.32 and −2.08 eV), revealing its preferential interaction with the (002) facet and thereby providing epitaxial deposition of Zn(002) facet. According to Bravais' law, the orientation of crystal facets is largely determined by the ion deposition rates on different facets. The crystallographic facets that are ultimately exposed typically have the lowest growth rates, while the faster-growing facets become to disappear. Therefore, the lowest Zn deposition rate on the Zn(002) facet facilitates their orderly stacking in the TFPM/ZSO electrolyte.

© 2025 Wiley-VCH GmbH

16163028, 2025, 47, Downloaded from https://advanced.onlinelibrary.wiley.com/doi/10.1002/adfm.202509705 by Tongji University, Wiley Online Library on [24/12/2025]. See the Terms and Conditions (https://onlinelibrary.wiley.com/terms-and-conditions) on Wiley Online Library for rules of use; OA articles are governed by the applicable Creative Commons License

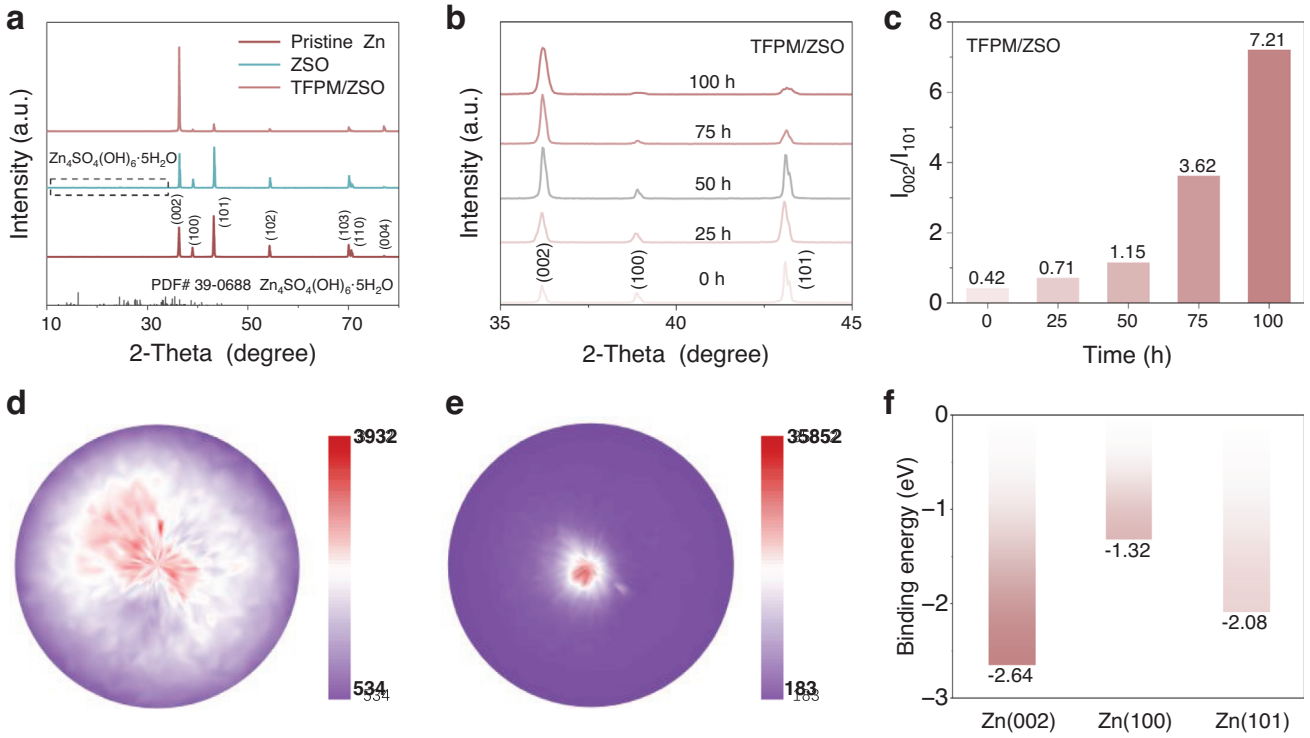

Figure 3. a) XRD patterns of Zn anodes after cycling in different electrolytes. b) XRD patterns of Zn anodes after cycling in TFPM/ZSO electrolyte for different times. c) The intensity ratio between the (002) and (101) facets. X-ray diffraction (002) pole figures of the Zn deposits in ZSO d) and TFPM/ZSO e) electrolytes. f) The adsorption energy of $TFPM^+$ on the Zn (002), (100), (101) facets.

Figure 4a shows the morphological evolution of Zn deposition at a current density of 4 mA cm^{-2}, random and irregular Zn particles are distributed on the anode surface in the ZSO electrolyte. The TFPM/ZSO electrolyte enables uniform and dense Zn deposits, and the hexagon-shaped Zn plates with layered stacking correspond to Zn(002) facets (Figure 4b). As shown in Figure 4c,d, digital photographs of Zn metal exhibit distinct color differences after electrodeposition at a current density of 10 mA cm^{-2} for 1 h in different electrolytes, which can serve as an indicator for determining the compactness of the Zn deposition. In the ZSO electrolyte, the black Zn surface is due to its loose and porous deposits (Figure 4e), and the gray Zn surface from the TFPM/ZSO electrolyte is attributed to the compact and homogeneous deposition topography (Figure 4f). The cross–sectional images in Figure 4g,h, show the disordered and random deposition with a thicker deposition layer in the ZSO electrolyte, while the TFPM/ZSO electrolyte renders a flat and dense deposition layer. In situ optical microscopies are shown in Figure 4i,j, a random spot-like distribution appears after 10 min in ZSO electrolyte, which gradually evolves into large and isolated Zn dendrites with an increased deposition time to 30 min. In TFPM/ZSO electrolyte, the Zn deposition maintains a flat surface without any dendrites in the whole evolution process, verifying that $TFPM^+$ regulates the deposition of zinc ions to suppress the tip effect by homogenizing the local surface electric field as verified by Zeta potential and differential capacitance results. In addition, the lower LUMO energy level of $TFPM^+$ mentioned in Figure 2a suggests that it is easy to gain electrons and undergo reduction during the deposition process in comparison with water. In the transmission electron microscope (TEM) images (Figure 4k,l), the interplanar spacing matches well with the (200) and (101) facets of ZnF_2, it is also confirmed by the binding energy of Zn $2p_{3/2}$ peak (1022.7 eV) in XPS results (Table S1). Energy dispersive spectroscopy (EDS) mapping further verifies that the elemental composition of the SEI originates from the $TFPM^+$(Figure 4m and Figure S9).

The reversibility and stability of Zn^{2+} plating–stripping were evaluated using Zn//Zn symmetric and Zn//Cu asymmetric batteries under different current densities. Figure S10 shows the rate performance of the symmetric batteries with/without TFPM at various current densities ranging from 0.5 to 10 mA cm^{-2}. The battery tested in the TFPM/ZSO electrolyte shows a steadier voltage profile than that in the ZSO electrolyte. When the current density returned to 0.5 mA cm^{-2}, the battery with TFPM/ZSO electrolyte continued to operate, whereas the battery with ZSO electrolyte failed. As shown in **Figure** 5a, the battery with ZSO electrolyte short-circuits after 300 h at a current density of 0.5 mA cm^{-2} with an areal capacity of 0.5 mAh cm^{-2}, while the battery with TFPM/ZSO electrolyte exhibits a stable cycle over 5900 h with a steady voltage hysteresis. The symmetric battery also achieves a cycle life of 3300 h within TFPM/ZSO electrolyte under a current density of 1 mA cm^{-2} and an areal capacity of 1 mAh cm^{-2} (Figure S11). Increasing the current density to 4 mA cm^{-2} with an areal capacity of 2 mAh cm^{-2}, the symmetric battery with TFPM/ZSO electrolyte can stably cycle for more than 1900 h, superior to 100 h of the battery with bare ZSO electrolyte (Figure 5b). Even after being cycled under harsh conditions of 10 mA cm^{-2} and 5 mAh cm^{-2}, a symmetric battery with

© 2025 Wiley-VCH GmbH

16163028, 2025, 47, Downloaded from https://advanced.onlinelibrary.wiley.com/doi/10.1002/adfm.202509705 by Tongji University, Wiley Online Library on [24/12/2025]. See the Terms and Conditions (https://onlinelibrary.wiley.com/terms-and-conditions) on Wiley Online Library for rules of use; OA articles are governed by the applicable Creative Commons License

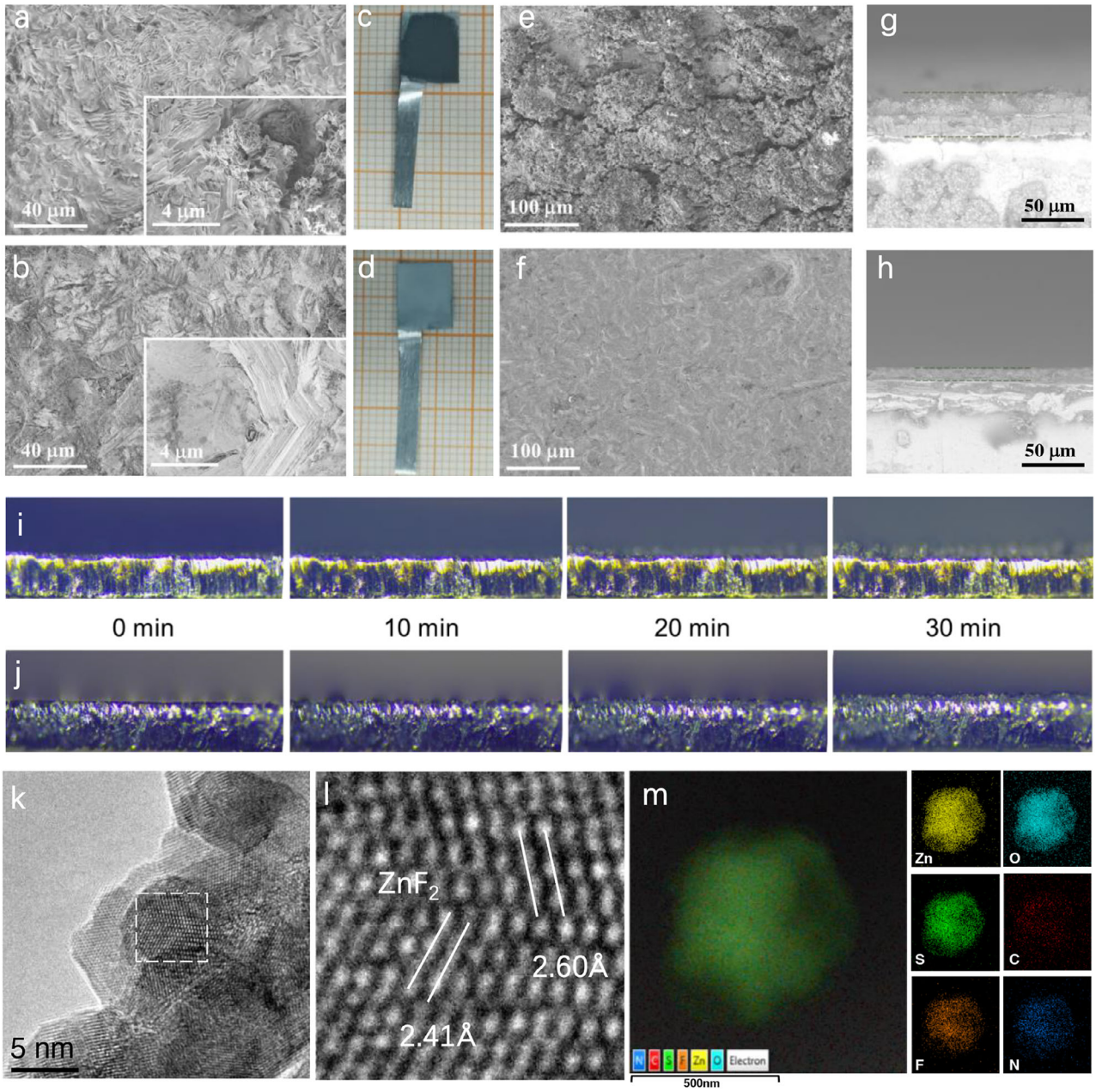

Figure 4. SEM images of Zn anodes after cycling in ZSO (a) and TFPM/ZSO (b) electrolytes at a current density of 4 mA cm^{-2} for 100 h. Digital photographs, surface, and cross–section SEM images of Zn metal after electroplated in ZSO (c), (e), (g) and TFPM/ZSO electrolytes (d), (f), (h) at a current density of 10 mA cm^{-2} for 1 h, respectively. In situ optical microscopic observations of Zn deposition in the ZSO (i) and TFPM/ZSO (j) electrolytes at a current density of 10 mA cm^{-2}. k–l) The high-resolution TEM images of the deposited Zn with SEI. m) The corresponding EDS-mapping results of Zn, O, C, S, N, and F elements.

TFPM/ZSO electrolyte still exhibits stable voltage polarization and high cycling stability for over 640 h. Conversely, a symmetric battery with ZSO electrolyte fails quickly due to an increased polarization after only a few cycles (Figure 5c). In addition, the cumulative plated capacity (CPC) in this work is superior to most works adopting the electrolyte modification strategy (Figure 5d).

The Zn//Cu asymmetric battery with the TFPM/ZSO electrolyte delivers an ultrahigh CE of 99.91% for 400 cycles at the current density of 5 mA cm^{-2}, more stable than that in the bare ZSO electrolyte (Figure S12). At a current density of 1 mA cm^{-2}, the asymmetric battery with TFPM/ZSO electrolyte exhibits an ultralong cycle number of 4000 times and an ultrahigh average CE of 99.93%, whereas the battery with the ZSO electrolyte fails after several cycles due to the short circuit induced by the Zn dendrites (Figure 5e and Figure S13). Benefiting from the regulation of the EDL structure by the TFPM additive, it isolates highly reactive water from contact with the zinc anode, effectively preventing the occurrence of side reactions. This significantly reduces the

© 2025 Wiley-VCH GmbH

16163028, 2025, 47, Downloaded from https://advanced.onlinelibrary.wiley.com/doi/10.1002/adfm.202509705 by Tongji University, Wiley Online Library on [24/12/2025]. See the Terms and Conditions (https://onlinelibrary.wiley.com/terms-and-conditions) on Wiley Online Library for rules of use; OA articles are governed by the applicable Creative Commons License

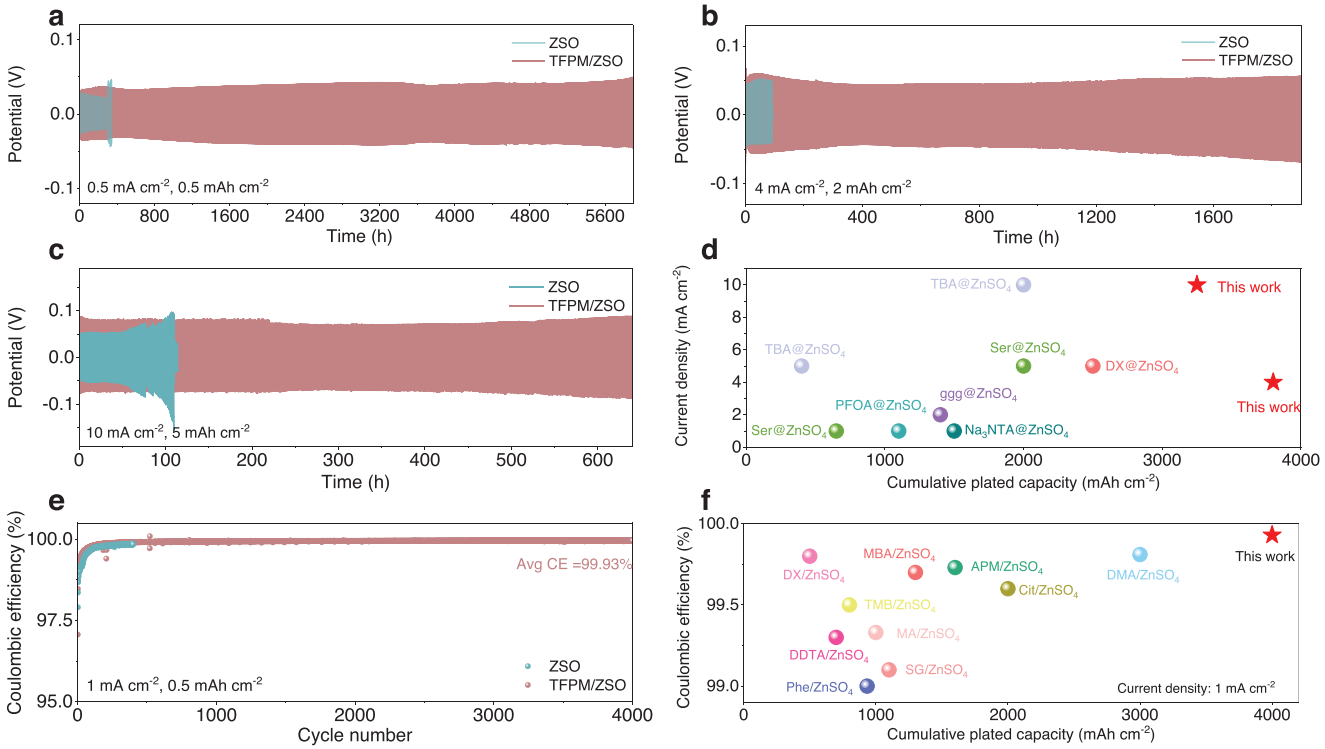

Figure 5. Voltage profiles of Zn//Zn symmetric batteries at various current densities and area capacity combinations of (a) 0.5 mA cm^{-2} and 0.5 mAh cm^{-2}; (b) 4 mA cm^{-2} and 2 mAh cm^{-2}; c) 10 mA cm^{-2} and 5 mAh cm^{-2}. d) Comparison in CPC of Zn//Zn batteries among AZIBs aiming advancements by electrolyte modification.[10a,c,15c,21] (e) CE of Zn//Cu asymmetric batteries at 1 mA cm^{-2} and 0.5 mAh cm^{-2}. f) Comparison in CE and CPC of Zn//Cu batteries with current advancements from electrolyte modification and SEI engineering at a current density of 1 mA cm^{-2}.[10b,c,15e,22]

irreversible consumption of the zinc anode, leading to a substantial improvement in Coulombic efficiency. Figure 5f and Table S2 demonstrate the great enhancements in CE and CPC in this work in comparison with other works by electrolyte modification, demonstrating the promising prospect of the TFPM additive.

Paring with MnVO synthesized through a hydrothermal method,[23] full batteries were assembled using electrolytes with and without TFPM additive. **Figure 6a** shows the charge/discharge curves, Zn//MnVO full battery with TFPM/ZSO electrolyte achieves a higher specific capacity of 311 mAh g^{-1} compared with 256 mAh g^{-1} from bare ZSO electrolyte at 4 A g^{-1}. The full battery using TFPM/ZSO electrolyte exhibits less polarization as reflected by the dQ/dV curves. In contrast, the full battery using ZSO electrolyte demonstrates progressively intensified polarization with prolonged cycling (Figure 6b and Figure S14). The Nyquist plots in Figure 6c show that the full battery with TFPM/ZSO electrolyte exhibits a lower reactive resistance compared to its counterpart, indicating improved ionic transfer and faster electron transport kinetics. Moreover, the full battery with TFPM/ZSO electrolyte delivers batter rate performance compared with the full battery using bare ZSO electrolyte (Figure 6d). At 0.5 A g^{-1}, a high capacity of 410 mAh g^{-1} is achieved in the TFPM/ZSO electrolyte. The current density increases to 8 A g^{-1}, and the specific capacity keeps at 260 mAh g^{-1}, while a full battery using bare ZSO electrolyte only achieves 210 mAh g^{-1}. For the self-discharge evaluation, the full battery with the TFPM/ZSO electrolyte shows higher voltage of 1.34 V and a higher capacity retention of 98.1% than that in the ZSO electrolyte (1.07 V and 69.6%) after resting for 24 h (Figure 6e), demonstrating the alleviated side reaction and suppressed self-discharge from TFPM additive. The cycling performance was also tested at a current density of 8 A g^{-1} (Figure 6f). Benefiting from the construction of an H_2O-poor EDL, the polarization is effectively reduced, while anode failure induced by dendrite growth and side reactions is prevented, the full battery with TFPM/ZSO electrolyte delivers a high reversible capacity of 263 mAh g^{-1} with a capacity retention of 94.9% over 6000 cycles and nearly 100% CE, higher than specific capacity of 217 mAh g^{-1} and capacity retention of 76.1% over 1700 cycles in bare ZSO electrolyte.

3. Conclusions

A series of organics with N-, phenyl-, and F- groups individually or jointly were systematically investigated to reveal their synergistic effects on the reversibility and stability of Zn anode in aqueous zinc ion batteries. The additive, TFPM, with the hydrophobic groups of benzene ring and fluorine together, has been proven to be the best interfacial stabilizer at the Zn anode- electrolyte interface due to its strong affinity to zinc. $TFPM^+$ with fluorinated aromatic groups isolate the active water molecule from the Zn anode surface, leading to the formation of H_2O-poor EDL, and preventing the side reactions between water and the zinc anode. Additionally, the adsorbed $TFPM^+$ regulates the diffusion of Zn ions at the anode-electrolyte interface to induce preferred

© 2025 Wiley-VCH GmbH

16163028, 2025, 47, Downloaded from https://advanced.onlinelibrary.wiley.com/doi/10.1002/adfm.202509705 by Tongji University, Wiley Online Library on [24/12/2025]. See the Terms and Conditions (https://onlinelibrary.wiley.com/terms-and-conditions) on Wiley Online Library for rules of use; OA articles are governed by the applicable Creative Commons License

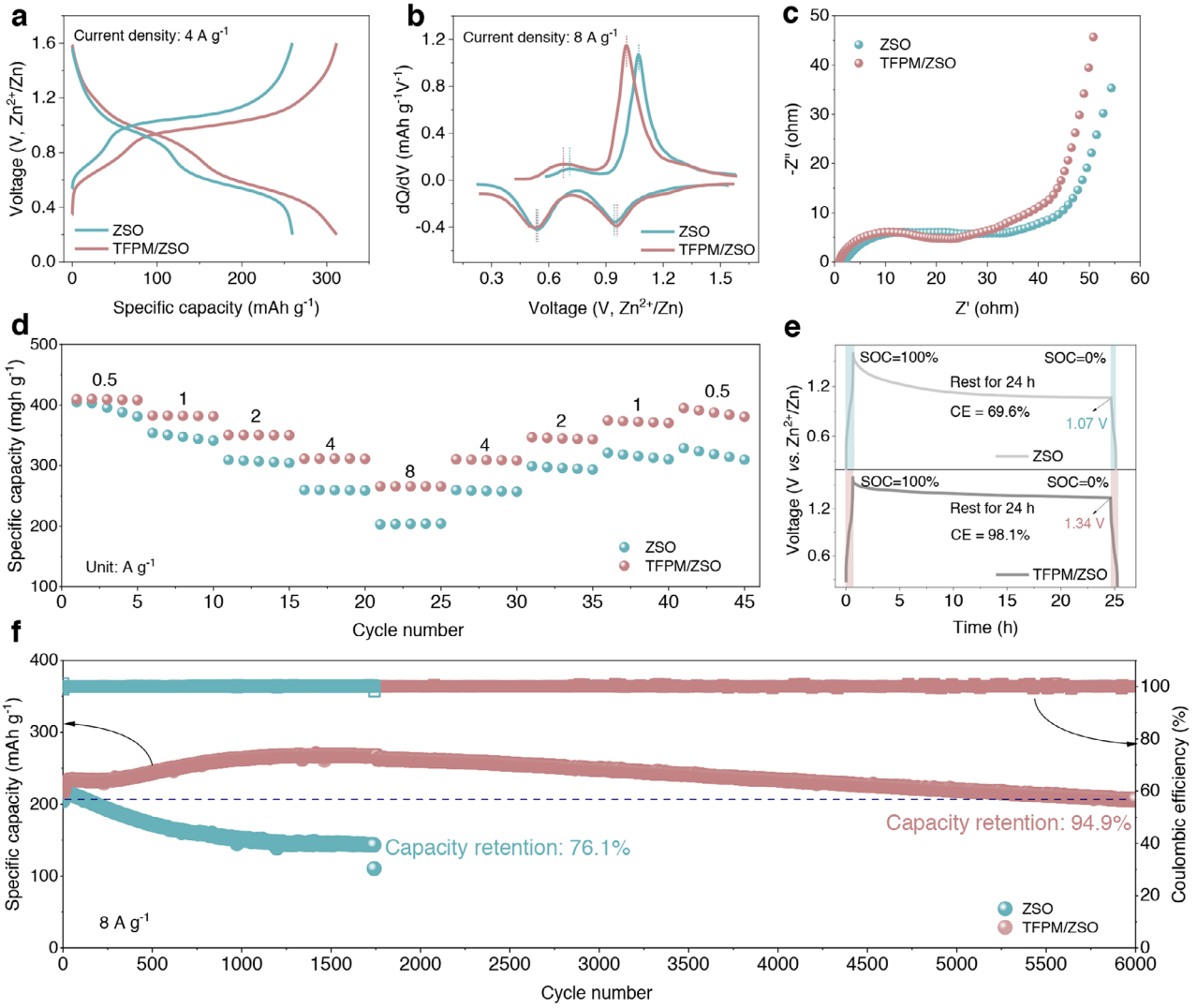

Figure 6. a) Charge–discharge curves of full batteries with different electrolytes at a current density of 4 A g^{-1}. b) dQ/dV curves of 1st cycle of full batteries with different electrolytes at a current density of 8 A g^{-1}. c) Electrochemical impedance spectroscopy (EIS) plots. d) Rate performance. e) Self-discharge curves. f) Long-term cycling performance at 8 A g^{-1}.

Zn(002) texture, and the ZnF_2-rich SEI formed from partial $TFPM^+$ decomposition further inhibits subsequent side reactions and dendrite formation. As a result, Zn//Zn symmetric batteries using TFPM additive deliver an ultralong cycle life of 5900 h at 0.5 mA cm^{-2}, and a high CE of 99.93% at a current density of 1 mA cm^{-2} in Zn//Cu asymmetric batteries over 4000 h. More importantly, Zn full batteries paring with Mn^{2+} preintercalated $V_2O_5{\cdot}nH_2O$ cathode exhibit higher cycle stability in the TFPM/ZSO electrolyte than that in bare ZSO electrolyte. This work provides a promising interface-engineering strategy from the functional group design of additives for high-performance aqueous zinc ion batteries.

Supporting Information

Supporting Information is available from the Wiley Online Library or from the author.

Acknowledgements

T.S. and C.L. contributed equally to this work. This work was financially supported by the National Natural Science Foundation of China (52102277, 52472238) and the Fundamental Research Funds for the Central Universities, conducted by Tongji University.

Conflict of Interest

The authors declare no conflict of interest.

Data Availability Statement

The data that support the findings of this study are available from the corresponding author upon reasonable request.

© 2025 Wiley-VCH GmbH

16163028, 2025, 47, Downloaded from https://advanced.onlinelibrary.wiley.com/doi/10.1002/adfm.202509705 by Tongji University, Wiley Online Library on [24/12/2025]. See the Terms and Conditions (https://onlinelibrary.wiley.com/terms-and-conditions) on Wiley Online Library for rules of use; OA articles are governed by the applicable Creative Commons License

Keywords

aqueous zinc-ion battery, EDL structure, fluorinated aromatic additive, solid electrolyte interphase, zinc-electrolyte interface

Received: April 17, 2025
Revised: May 14, 2025
Published online: November 3, 2025

[1] a) J. Zheng, Q. Zhao, T. Tang, J. Yin, C. D. Quilty, G. D. Renderos, X. Liu, Y. Deng, L. Wang, D. C. Bock, C. Jaye, D. Zhang, E. S. Takeuchi, K. J. Takeuchi, A. C. Marschilok, L. A. Archer, *Science* **2019**, *366*, 645; b) C. Yang, J. Xia, C. Cui, T. P. Pollard, J. Vatamanu, A. Faraone, J. A. Dura, M. Tyagi, A. Kattan, E. Thimsen, J. Xu, W. Song, E. Hu, X. Ji, S. Hou, X. Zhang, M. S. Ding, S. Hwang, D. Su, Y. Ren, X. Q. Yang, H. Wang, O. Borodin, C. Wang, *Nat. Sustainability* **2023**, *6*, 325; c) W. Sun, F. Wang, B. Zhang, M. Zhang, V. Küpers, X. Ji, C. Theile, P. Bieker, K. Xu, C. Wang, M. Winter, *Science* **2021**, *371*, 46; d) R. F. Service, *Science* **2021**, *372*, 890; e) L. E. Blanc, D. Kundu, L. F. Nazar, *Joule* **2020**, *4*, 771.

[2] a) C. Zhong, B. Liu, J. Ding, X. Liu, Y. Zhong, Y. Li, C. Sun, X. Han, Y. Deng, N. Zhao, W. Hu, *Nat. Energy* **2020**, *5*, 440; b) L. Cao, D. Li, T. Pollard, T. Deng, B. Zhang, C. Yang, L. Chen, J. Vatamanu, E. Hu, M. J. Hourwitz, L. Ma, M. Ding, Q. Li, S. Hou, K. Gaskell, J. T. Fourkas, X. Q. Yang, K. Xu, O. Borodin, C. Wang, *Nat. Nanotechnol.* **2021**, *16*, 902; c) L. Ma, M. A. Schroeder, O. Borodin, T. P. Pollard, M. S. Ding, C. Wang, K. Xu, *Nat. Energy* **2020**, *5*, 743; d) D. Chao, W. Zhou, F. Xie, C. Ye, H. Li, M. Jaroniec, S. Z. Qiao, *Sci. Adv.* **2020**, *6*, aba4098.

[3] a) J. Cao, D. Zhang, C. Gu, X. Wang, S. Wang, X. Zhang, J. Qin, Z. S. Wu, *Adv. Energy Mater.* **2021**, *11*, 2101299; b) J. Zheng, L. A. Archer, *Chem. Rev.* **2022**, *122*, 14440; c) S. Wu, Z. Hu, P. He, L. Ren, J. Huang, J. Luo, *eScience* **2023**, *3*, 100120.

[4] a) Y. Zhu, G. Liang, X. Cui, X. Liu, H. Zhong, C. Zhi, Y. Yang, *Energy Environ. Sci.* **2024**, *17*, 369; b) X. Li, X. Wang, L. Ma, W. Huang, *Adv. Energy Mater.* **2022**, *12*, 2202068; c) S. Liu, J. Mao, W. K. Pang, J. Vongsvivut, X. Zeng, L. Thomsen, Y. Wang, J. Liu, D. Li, Z. Guo, *Adv. Funct. Mater.* **2021**, *31*, 2104281.

[5] R. Zhao, Y. Yang, G. Liu, R. Zhu, J. Huang, Z. Chen, Z. Gao, X. Chen, L. Qie, *Adv. Funct. Mater.* **2021**, *31*, 2001867.

[6] L. Yang, M. Zhou, Y. Xie, X. Shen, S. Liang, G. Fang, *Energy Storage Mater.* **2024**, *67*, 103271.

[7] a) Z. Yi, J. Liu, S. Tan, Z. Sang, J. Mao, L. Yin, X. Liu, L. Wang, F. Hou, S. X. Dou, H. M. Cheng, J. Liang, *Adv. Mater.* **2022**, *34*, 2203835; b) Y. Yan, C. Shu, T. Zeng, X. Wen, S. Liu, D. Deng, Y. Zeng, *ACS Nano* **2022**, *16*, 9150; c) T. Shen, T. Wei, S. Zhang, H. Liu, C. Li, Z. Li, M. Yang, C. Liu, Y. Pei, *Small Struct.* **2025**, *6*, 2400325.

[8] Z. Zhao, R. Wang, C. Peng, W. Chen, T. Wu, B. Hu, W. Weng, Y. Yao, J. Zeng, Z. Chen, P. Liu, Y. Liu, G. Li, J. Guo, H. Lu, Z. Guo, *Nat. Commun.* **2021**, *12*, 6606.

[9] T. Wang, C. Li, X. Xie, B. Lu, Z. He, S. Liang, J. Zhou, *ACS Nano* **2020**, *14*, 16321.

[10] a) Y. Wang, L. e. Mo, X. Zhang, Y. Ren, T. Wei, Z. Li, Y. Huang, H. Zhang, G. Cao, L. Hu, *Adv. Energy Mater.* **2023**, *13*, 2301517; b) T. Wei, H. Zhang, Y. Ren, L. e. Mo, Y. He, P. Tan, Y. Huang, Z. Li, D. Zhu, L. Hu, *Adv. Funct. Mater.* **2024**, *34*, 2312506; c) T. Wei, Y. Ren, Y. Wang, L. e. Mo, Z. Li, H. Zhang, L. Hu, G. Cao, *ACS Nano* **2023**, *17*, 3765.

[11] Y. Geng, L. Pan, Z. Peng, Z. Sun, H. Lin, C. Mao, L. Wang, L. Dai, H. Liu, K. Pan, X. Wu, Q. Zhang, Z. He, *Energy Storage Mater.* **2022**, *51*, 733.

[12] D. M. Xu, X. T. Ren, H. Y. Li, Y. R. Zhou, S. M. Chai, Y. N. Chen, H. Li, L. S. Bai, Z. Chang, A. Q. Pan, H. S. Zhou, *Angew. Chem., Int. Ed.* **2024**, *136*, 202402833.

[13] a) Y. Lv, M. Zhao, Y. Du, Y. Kang, Y. Xiao, S. Chen, *Energy Environ. Sci.* **2022**, *15*, 4748; b) W. Xu, J. Li, X. Liao, L. Zhang, X. Zhang, C. Liu, K. Amine, K. Zhao, J. Lu, *J. Am. Chem. Soc.* **2023**, *145*, 22456; c) Y. Dai, R. Lu, C. Zhang, J. Li, Y. Yuan, Y. Mao, C. Ye, Z. Cai, J. Zhu, J. Li, R. Yu, L. Cui, S. Zhao, Q. An, G. He, G. I. N. Waterhouse, P. R. Shearing, Y. Ren, J. Lu, K. Amine, Z. Wang, L. Mai, *Nat. Catal.* **2024**, *7*, 776.

[14] a) Y. Zhong, Z. Cheng, H. Zhang, J. Li, D. Liu, Y. Liao, J. Meng, Y. Shen, Y. Huang, *Nano Energy* **2022**, *98*, 107220; b) D. Q. Cai, H. Cheng, J. L. Yang, H. Liu, T. Xiao, X. Liu, M. Chen, H. J. Fan, *Energy Environ. Sci.* **2024**, *17*, 8349.

[15] a) T. Li, S. Hu, C. Wang, D. Wang, M. Xu, C. Chang, X. Xu, C. Han, *Angew. Chem., Int. Ed.* **2023**, *62*, 202314883; b) M. Wu, X. Wang, F. Zhang, Q. Xiang, Y. Li, J. Guo, *Energy Environ. Sci.* **2024**, *17*, 619; c) J. Zhang, Y. Liu, Y. Wang, Z. Zhu, Z. Yang, *Adv. Funct. Mater.* **2024**, *34*, 2401889; d) C. Li, A. Shyamsunder, A. G. Hoane, D. M. Long, C. Y. Kwok, P. G. Kotula, K. R. Zavadil, A. A. Gewirth, L. F. Nazar, *Joule* **2022**, *6*, 1103; e) Q. Zong, Y. Yu, C. Liu, Q. Zhang, G. Wei, J. Wang, J. Zhang, G. Cao, *ACS Nano* **2024**, *18*, 27440.

[16] Y. Ni, L. Lin, Y. Shang, L. Luo, L. Wang, Y. Lu, Y. Li, Z. Yan, K. Zhang, F. Cheng, J. Chen, *Angew. Chem., Int. Ed.* **2021**, *60*, 16937.

[17] a) Y. Wu, Z. Zhu, D. Shen, L. Chen, T. Song, T. Kang, Z. Tong, Y. Tang, H. Wang, C. S. Lee, *Energy Storage Mater.* **2022**, *45*, 1084; b) L. Liu, H. Lu, C. Han, X. Chen, S. Liu, J. Zhang, X. Chen, X. Wang, R. Wang, J. Xu, H. K. Liu, S. X. Dou, W. Li, *ACS Nano* **2023**, *17*, 23065; c) C. Huang, X. Zhao, S. Liu, Y. Hao, Q. Tang, A. Hu, Z. Liu, X. Chen, *Adv. Mater.* **2021**, *33*, 2100445.

[18] a) J. Zhou, M. Xie, F. Wu, Y. Mei, Y. Hao, R. Huang, G. Wei, A. Liu, L. Li, R. Chen, *Adv. Mater.* **2021**, *33*, 2101649; b) X. Guo, J. Lu, M. Wang, A. Chen, H. Hong, Q. Li, J. Zhu, Y. Wang, S. Yang, Z. Huang, Y. Wang, Z. Pei, C. Zhi, *Chem* **2024**, *10*, 3607.

[19] a) Y. Zhang, S. Shen, K. Xi, P. Li, Z. Kang, J. Zhao, D. Yin, Y. Su, H. Zhao, G. He, S. Ding, *Angew. Chem., Int. Ed.* **2024**, *63*, 202407067; b) S. Tian, T. Hwang, Z. Zhang, S. Wu, A. Mashhadian, R. Zhang, T. Milazzo, T. Luo, R. Jian, T. Li, K. Cho, G. Xiong, *ACS Nano* **2025**, *19*, 3135; c) K. Zhou, G. Liu, X. Zhu, G. Liu, X. Yu, Z. Guo, Y. Wang, *Angew. Chem., Int. Ed.* **2025**, *64*, 202413959.

[20] L. Ma, Q. Li, Y. Ying, F. Ma, S. Chen, Y. Li, H. Huang, C. Zhi, *Adv. Mater.* **2021**, *33*, 2007406.

[21] a) A. Bayaguud, X. Luo, Y. Fu, C. Zhu, *ACS Energy Lett.* **2020**, *5*, 3012; b) M. Qiu, P. Sun, Y. Wang, L. Ma, C. Zhi, W. Mai, *Angew. Chem., Int. Ed.* **2022**, *61*, 202210979; c) F. Zhao, Z. Jing, X. Guo, J. Li, H. Dong, Y. Tan, L. Liu, Y. Zhou, R. Owen, P. R. Shearing, D. J. L. Brett, G. He, I. P. Parkin, *Energy Storage Mater.* **2022**, *53*, 638.

[22] a) B. Niu, Z. Li, D. Luo, X. Ma, Q. Yang, Y. E. Liu, X. Yu, X. He, Y. Qiao, X. Wang, *Energy Environ. Sci.* **2023**, *16*, 1662; b) C. Li, G. Qu, X. Zhang, C. Wang, X. Xu, *Energy Environ. Mater.* **2024**, *7*, 12608; c) Z. Zha, T. Sun, D. Li, T. Ma, W. Zhang, Z. Tao, *Energy Storage Mater.* **2024**, *64*, 103059; d) J. Hao, L. Yuan, Y. Zhu, M. Jaroniec, S. Z. Qiao, *Adv. Mater.* **2022**, *34*, 2206963; e) J. Chen, N. Liu, W. Dong, Y. Xu, Y. Cao, S. Zhang, J. Hou, H. Bi, T. Lin, F. Q. Huang, *Adv. Funct. Mater.* **2024**, *34*, 2313925; f) T. Yan, M. Tao, J. Liang, G. Zheng, B. Wu, L. Du, Z. Cui, H. Song, *Energy Storage Mater.* **2024**, *65*, 103190; g) A. Zhou, H. Wang, F. Zhang, X. Hu, Z. Song, Y. Chen, Y. Huang, Y. Cui, Y. Cui, L. Li, F. Wu, R. Chen, *Nano-Micro Lett.* **2024**, *16*, 164; h) Y. Li, L. Liu, H. Zhang, H. Wang, Z. Sun, Z. Zhang, W. Pang, S. Omanovic, S. Sun, X. Chen, H. Song, *Adv. Funct. Mater.* **2025**, *35*, 2410855.

[23] C. Liu, Z. Neale, J. Zheng, X. Jia, J. Huang, M. Yan, M. Tian, M. Wang, J. Yang, G. Cao, *Energy Environ. Sci.* **2019**, *12*, 2273.

© 2025 Wiley-VCH GmbH

16163028, 2025, 47, Downloaded from https://advanced.onlinelibrary.wiley.com/doi/10.1002/adfm.202509705 by Tongji University, Wiley Online Library on [24/12/2025]. See the Terms and Conditions (https://onlinelibrary.wiley.com/terms-and-conditions) on Wiley Online Library for rules of use; OA articles are governed by the applicable Creative Commons License